Supplemental Material for
Observation of Quantum Temporal Correlations
Well Beyond Lüders Bound

Chun-Wang Wu,[1,2] Man-Chao Zhang,[1,2] Yan-Li Zhou,[1,2] Ting Chen,[1,2] Ran Huang,[3] Yi Xie,[1,2] Wen-bo Su,[1,2] Bao-Quan Ou,[1,2] Wei Wu,[1,2,4] Adam Miranowicz,[3,5] Franco Nori,[3] Jie Zhang,[1,2,*] Hui Jing,[6,†] and Ping-Xing Chen[1,2,4,‡]

[1] *Institute for Quantum Science and Technology, College of Science, NUDT, Changsha 410073, Hunan, China*
[2] *Hunan Key Laboratory of Quantum Information Mechanism and Technology, NUDT, Changsha 410073, Hunan, China*
[3] *Quantum Computing Center and Cluster for Pioneering Research, RIKEN, Wako-shi, Saitama 351-0198, Japan*
[4] *Hefei National Laboratory, Hefei 230088, Anhui, China*
[5] *Institute of Spintronics and Quantum Information, Faculty of Physics, Adam Mickiewicz University, 61-614 Poznań, Poland*
[6] *Department of Physics and Synergetic Innovation Center for Quantum Effects and Applications, Hunan Normal University, Changsha, China*

(Dated: December 27, 2024)

In this Supplemental Material, we describe in more detail our experimental techniques used. Moreover, we also provide a detailed theoretical analysis of quantum temporal correlations (QTCs) in our parity-time ($\mathcal{PT}$)-symmetric model.

I. EXPERIMENTAL TECHNIQUES

A. Initial state preparation and evolution operator decomposition

A constant magnetic field of 5.3 G splits the adjacent Zeeman sublevels of $S_{1/2}$ and $D_{5/2}$ by $2\pi\times$ 14.8 MHz and $2\pi\times$ 8.9 MHz, respectively, making the different S-D transitions frequency selective. A narrow linewidth, linearly polarized 729 nm laser is used to coherently drive the trapped ion, with a 45° angle between the laser wave vector $\vec{k}$ and the magnetic field $\vec{B}$. The polarization direction of the laser forms a 65° angle with the $\vec{k}$-$\vec{B}$ plane. The target S-D transition can be addressed by adjusting the detuning between the laser frequency and the atomic frequency to zero. The associated Rabi frequency, Ω_R, is set to about $2\pi\times$ 10 KHz, which can be calibrated by experimentally fitting the Rabi oscillation. Then, the resonant coupling between each pair of the four Zeeman sublevels can be described by the equatorial rotations

$$R_{ij}(\theta,\phi)=\exp\Big\{-i\theta[\cos(\phi)\sigma_x^m+\sin(\phi)\sigma_y^m]/2\Big\}, \tag{S1}$$

where i and j indicate the addressed transition, σ_x^m, σ_y^m are the Pauli x, y matrices in the representation of $\hat{\sigma}_z$, and $\theta=\Omega_R t$ is the rotation angle. The rotation phase ϕ is the laser phase when $|i\rangle$ is in the S manifold, but we need to add a negative sign when $|j\rangle$ is in the S state.

Taking advantage of the above elementary operations and the decomposition method described in Ref. [1], the initial state preparation and unitary evolutionary operation in our experiment can be realized by applying an appropriate series of S-D equatorial rotations. All the state preparation starts from the same state $|1\rangle=(1,0,0,0)^T$. We introduce the metric operator $\eta=\frac{1}{\Omega}[J,-i\Gamma;i\Gamma,J]$ for $\hat{H}_{\rm PT}$ [2], where J and Γ are the coupling and loss (gain) rates of our $\mathcal{PT}$-symmetric system, and $\Omega=\sqrt{J^2-\Gamma^2}$ denotes the effective oscillation frequency. To simplify the mathematical expressions, we define the parameter $\sin(\alpha)=\Gamma/J$. The initial states used in our experiment and their preparation sequences are summarized in Table I, where η means the metric operator we have introduced.

The dynamic evolution after the state preparation is described by a unitary operator $U(\alpha,\tau)$, which can be decomposed into four equatorial rotations in the experiment. The concrete form and experimental execution sequence of $U(\alpha,\tau)$ can be written as

* Corresponding author: zj1589233@126.com
† Corresponding author: jinghui@hunnu.edu.cn
‡ Corresponding author: pxchen@nudt.edu.cn

$$U(\alpha,\tau)=\begin{pmatrix}\cos(\tau) & -i\cos(\alpha)\sin(\tau) & \sin(\tau)\sin(\alpha) & 0\\ -i\cos(\alpha)\sin(\tau) & \cos(\tau) & 0 & -\sin(\tau)\sin(\alpha)\\ -\sin(\tau)\sin(\alpha) & 0 & \cos(\tau) & -i\cos(\alpha)\sin(\tau)\\ 0 & \sin(\tau)\sin(\alpha) & -i\cos(\alpha)\sin(\tau) & \cos(\tau)\end{pmatrix} \tag{S2}$$
$$= R_{23}(2\alpha,0)R_{12}(2\tau,0)R_{34}(2\tau,0)R_{23}(2\alpha,\pi),$$

where $\tau=\Omega t$ is the scaled time. For different ratios of Γ/J, we can achieve the corresponding $U(\alpha,\tau)$ by choosing the appropriate rotation angles and rotation phases for the sequence of equatorial rotations given in Eq. (S2).

B. State detection and population normalization

In the detection process, we only need to extract the populations of the states $|1\rangle$ and $|2\rangle$, which are labeled as p_1 and p_2. However, the populations may be distributed in the four states during the evolution. Two equatorial rotations and two fluorescence detection processes are employed to distinguish the states $|1\rangle$ and $|2\rangle$ from the subspace consisting of $|3\rangle$ and $|4\rangle$. The first step includes a π-pulse rotation $R_{14}(\pi,0)$ and a subsequent fluorescence detection; then another $R_{14}(\pi,0)$ is used to swap the states back and the fluorescence detection is applied again in the second step. Regarding the results obtained in above steps, the bright state in the first step denotes the population out of the subspace $\mathcal{H}_S=\{|1\rangle,|2\rangle\}$, the dark state in the first step combined with the bright state in the second step gives the population p_1, and the dark states in both steps give the result for p_2.

In the experiment, the total population $p=p_1+p_2$ for $\mathcal{H}_S$ exhibits periodic oscillatory behavior, which is a quantum version of the power oscillation phenomenon in classical $\mathcal{PT}$-symmetric system. By introducing the normalized populations $p_1^n=\frac{p_1}{p_1+p_2}$ and $p_2^n=\frac{p_2}{p_1+p_2}$, we can experimentally obtain the normalized dynamics of a $\mathcal{PT}$-symmetric qubit described by Eq. (3) of the main text.

TABLE I. Target initial states and the corresponding preparation sequences.

Unnormalized target initial state	Preparation sequence	State in figures
$\begin{pmatrix}0\\1\end{pmatrix}\oplus\eta\begin{pmatrix}0\\1\end{pmatrix}$	$R_{34}(\theta_2,\pi)\cdot R_{23}(\theta_1,0)\cdot R_{12}(\pi,0)$ $\theta_2=2\arccos\left(\frac{\tan(\alpha)}{\sqrt{\sec(\alpha)^2+\tan(\alpha)^2}}\right)$ $\theta_1=2\arccos\left(\frac{\cos(\alpha)}{\sqrt{2}}\right)$	
$\begin{pmatrix}1\\-i\end{pmatrix}\oplus\eta\begin{pmatrix}1\\-i\end{pmatrix}$	$R_{34}(\theta_2,\pi)\cdot R_{12}(\theta_1,0)\cdot R_{14}(\theta_0,0)$ $\theta_2=\pi/2$ $\theta_1=\pi/2$ $\theta_0=2\,\mathrm{arcsec}\left(\sqrt{1+(\sec(\alpha)-\tan(\alpha))^2}\right)$	Fig. 3 Fig. 4(a-d)
$\begin{pmatrix}1\\i\end{pmatrix}\oplus\eta\begin{pmatrix}1\\i\end{pmatrix}$	$R_{34}(\theta_2,0)\cdot R_{12}(\theta_1,\pi)\cdot R_{14}(\theta_0,\pi)$ $\theta_2=\pi/2$ $\theta_1=\pi/2$ $\theta_0=2\arctan(\tan(\alpha)+\sec(\alpha))$	Fig. 4(a-d)
$\begin{pmatrix}\cos(\gamma)-\sin(\gamma)\\-i\cos(\gamma)-i\sin(\gamma)\end{pmatrix}\oplus\eta\begin{pmatrix}\cos(\gamma)-\sin(\gamma)\\-i\cos(\gamma)-i\sin(\gamma)\end{pmatrix}$	$R_{34}(\theta_2,\pi)\cdot R_{12}(\theta_1,0)\cdot R_{14}(\theta_0,0)$ $\theta_2=2\arcsin\left(\frac{\cos(\gamma)-\sin(\gamma)-\sin(\alpha)(\cos(\gamma)+\sin(\gamma))}{\sqrt{3-\cos(2\alpha)-4\cos(2\gamma)\sin(\alpha)}}\right)$ $\theta_1=2\arccos\left(\frac{\cos(\gamma)-\sin(\gamma)}{\sqrt{2}}\right)$ $\theta_0=2\arccos\left(\frac{\cos(\alpha)}{\sqrt{2-2\cos(2\gamma)\sin(\alpha)}}\right)$ $\gamma=\arcsin\left(\sqrt{\frac{J-\Gamma}{2J}}\right)$	Fig. 4(f)

C. Quantum state tomography

To study the accelerated dynamics shown in Fig. 3, a quantum state tomography technique is used to study the dynamic evolution of the $\mathcal{PT}$-symmetric qubit, which can obtain the full information of the Bloch vector at each moment. The z component of the Bloch vector, denoted as $\langle\hat{\sigma}_z\rangle$, can be directly extracted by experimentally measuring the difference of the normalized populations p_1^n and p_2^n. The x (y) component, denoted as $\langle\hat{\sigma}_x\rangle$ ($\langle\hat{\sigma}_y\rangle$), can be obtained by the combination of an extra equatorial rotation $R_{12}(3\pi/2,\pi/2)$ [$R_{12}(\pi/2,0)$] and the following detection procedure of $\langle\hat{\sigma}_z\rangle$. Finally, the maximum likelihood estimation method is utilized to reduce the statistical and systematic errors.

II. MEASUREMENT OF THE CORRELATION FUNCTIONS

A. Prepare-and-measure scenario

In our experiments, we use the "prepare-and-measure scenario" [3] to obtain the QTCs, which has been employed before for studying the Leggett-Garg inequalities (LGIs) in nitrogen-vacancy (NV) centers [4], ions [5], and superconducting qubits [3]. In the following, we explain in detail this widely used method.

When the projection measurement is non-destructive, i. e., the system is left in the eigenstate corresponding to the measurement outcome, we use consecutive measurements to obtain two-time correlators (such procedure was named as "direct-measure scenario" in Ref. [3]). However, in practice, the projective measurements are usually destructive, failing to leave the system in the ideal eigenstate. Examples include fluorescence readout of the qubits encoded in NV centers [6] or in energy level of trapped ions [7], free induction decay in nuclear magnetic resonance (NMR) [8], as well as absorptive detection of photons [9]. To circumvent this obstacle, the prepare-and-measure scenario can be implemented in two equivalent procedures [3, 10, 11], see Fig. S1.

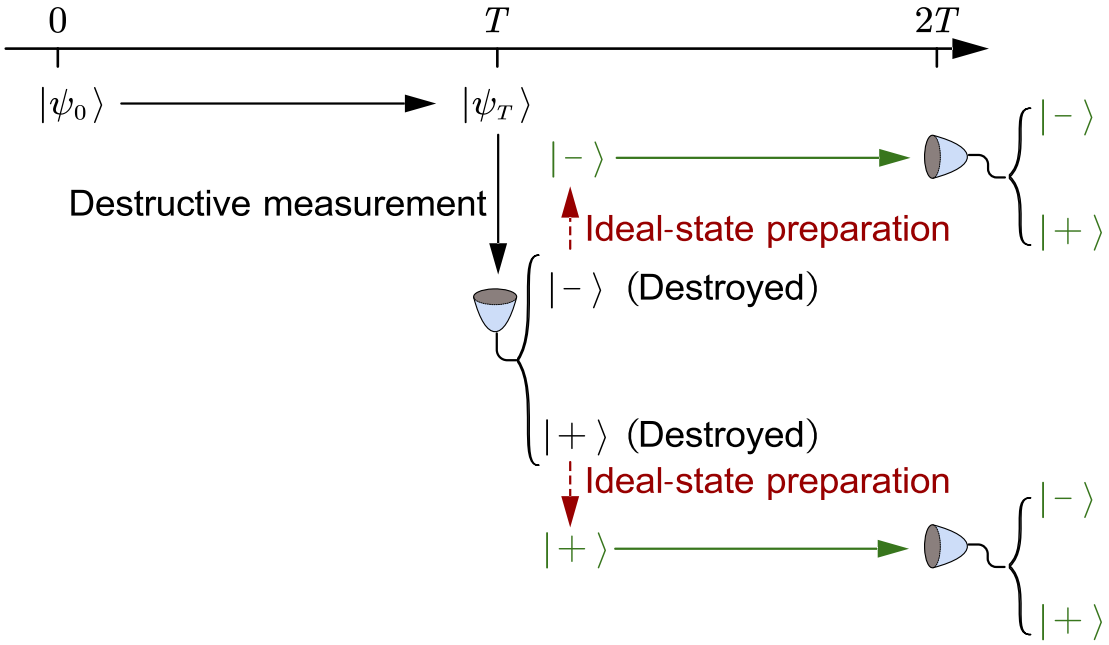

FIG. S1. The prepare-and-measure scenario.

First procedure: prepare the initial state $|\psi_0\rangle$ → perform the evolution for a period T → implement the intermediate destructive measurement, obtaining a measurement outcome but destroying the corresponding eigenstate → re-prepare the eigenstate corresponding to the outcome → continue to evolve for a period T → implement the second destructive measurement → repeat all the previous steps many times, then compute a desired two-time correlator.

Second equivalent procedure consists of three steps:

Step 1: prepare the initial state $|\psi_0\rangle$ → perform the evolution for a period T → implement the destructive measurement → repeat all the previous steps many times, then compute the conditional probabilities $p(-\mid\psi_0)$ and

$p(+\mid\psi_0)$.

Step 2: prepare the system in eigenstate $|-\rangle$ ($|+\rangle$) $\rightarrow$ perform the evolution for a period $T \rightarrow$ implement the destructive measurement $\rightarrow$ repeat all the previous steps many times, then compute the conditional probabilities $p(-\mid-)$ and $p(+\mid-)$ [$p(-\mid+)$ and $p(+\mid+)$].

Step 3: calculate the two-time correlator by combining these conditional probabilities.

The experimental scheme to obtain the two-time correlators in this work [i. e., Eq. (5) in main text] was designed according to the second procedure of the "prepare-and-measure scenario". It should be noted that, whether the studied system is classical or quantum, the "prepare-and-measure scenario" holds only on the premise of an "ideal-state preparation" (Fig. S1) [i. e. the re-prepared state is the same as the state left by measuring the system using an imaginary non-destructive measurement, more technical details can be found in Refs. [3, 10]].

The system considered in our experiment is a simple two-level system, which only consists of two distinguishable states, with the one-to-one correspondence between the measurement outcomes ($-$ and $+$) and the distinguishable states. Therefore, the premise of an "ideal-state preparation" is satisfied in our model, and the experimental method for obtaining the two-time correlators in this work is robust.

B. Experimental procedure for obtaining the quantum correlation functions

Our test of the LGI chooses three scaled time instants, labeled as $\tau_1 = 0$, $\tau_2 = T$ and $\tau_3 = 2T$. The two-time correlation functions, C_{12}, C_{13}, and C_{23}, can be indirectly measured via the conditional probability $p_\tau(Q^{'}|Q)$, for observing the measurement outcome $Q^{'}$ at the scaled time τ given that we deterministically initialize the qubit in the eigenstate $|Q\rangle$. In the experiment, $p_{_T}(+|-)$ [$p_{_{2T}}(+|-)$] is measured by preparing the initial state in $|-\rangle_y$, then applying the evolution operation $U(\alpha, T)$ [$U(\alpha, 2T)$], and finally measuring the probability distribution of the physical observable $\hat{\sigma}_y$. The conditional probabilities $p_{_T}(-|-)$ and $p_{_{2T}}(-|-)$ can be obtained by the normalization relations $p_{_T}(+|-) + p_{_T}(-|-) = 1$ and $p_{_{2T}}(+|-) + p_{_{2T}}(-|-) = 1$, respectively. Similar procedure is performed to obtain the conditional probabilities $p_{_T}(+|+)$ and $p_{_T}(-|+)$. Based on the above experimental data, C_{12}, C_{13}, and C_{23} can be obtained using Eq. (5) in the main text. In Fig. S2, we show our experimental results for the obtained conditional probabilities and the correlation functions, and the error bars are calculated by the binomial distributions of p_1^n and p_2^n.

III. MEASUREMENT OF THE QUANTUM WITNESS W

To measure the quantum witness

$$W = |p'(Q) - p(Q)| \tag{S3}$$

experimentally, $p'(Q)$ and $p(Q)$ should be addressed separately. The probability $p(Q)$, which indicates the probability for observing the outcome Q without earlier measurement, can be obtained by preparing the initial state

$$|\psi\rangle_0 = -\frac{\sqrt{J-\Gamma}}{\sqrt{2J}}|+\rangle_y + \frac{\sqrt{J+\Gamma}}{\sqrt{2J}}|-\rangle_y, \tag{S4}$$

then applying the evolution operation $U(\alpha, \tau = \pi/4)$, and finally measuring the normalized population $p_{y+}^n = \frac{\langle\hat{\sigma}_y\rangle+1}{2}$, where we have chosen $Q = 1$. However, obtaining the probability

$$p'(Q) = \sum_{Q_0=\pm1} p(Q|Q_0)p(Q_0) \tag{S5}$$

with an earlier measurement applied to the initial state requires several different measurement processes. The probability $p(Q_0 = +1)$ [$p(Q_0 = -1)$] is obtained by measuring $p_{y+}^n = \frac{\langle\hat{\sigma}_y\rangle+1}{2}$ ($p_{y-}^n = \frac{1-\langle\hat{\sigma}_y\rangle}{2}$) right after the initial state $|\psi\rangle_0$ is prepared. The conditional probability $p(Q = 1|Q_0 = +1)$ [$p(Q = 1|Q_0 = -1)$] requires the measurement of p_{y+}^n for the initial state $|+\rangle_y$ ($|-\rangle_y$) followed by the unitary evolution operator $U(\alpha, \tau = \pi/4)$. Experimental results for $p(Q)$, $p(Q_0) = \pm1$, and $p(Q = 1|Q_0 = \pm1)$ are shown in Fig. S3. The quantum witness W can be obtained using the definition of W in the main text.

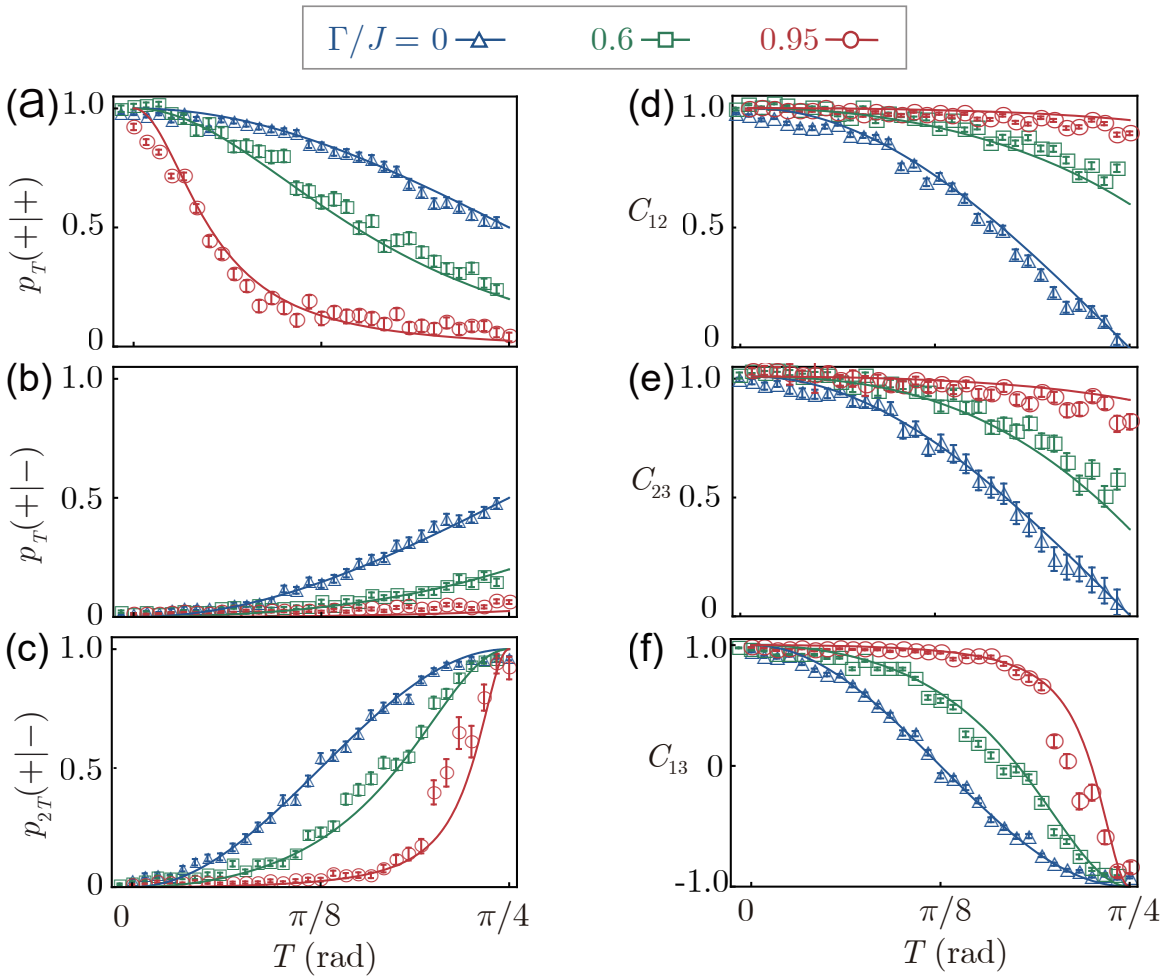

FIG. S2. (color online). Conditional probabilities and two-time correlation functions. [(a)-(c)] Measurement results of the conditional probabilities $p_T(+|+)$ (a), $p_T(+|-)$ (b), and $p_{2T}(+|-)$ (c) versus the measurement time interval T for $\Gamma/J = 0$, 0.6 and 0.95. [(d)-(f)] Correlation functions C_{12} (d), C_{23} (e), and C_{13} (f) versus the measurement time interval T for $\Gamma/J = 0$, 0.6 and 0.95. Error bars represent the standard deviation.

IV. CONSTRUCTION OF THE $\mathcal{PT}$-SYMMETRIC SYSTEM

A. Theoretical construction of the unitary operator $U(\alpha, \tau)$

According to the theory in Ref. [2], a $\mathcal{PT}$-symmetric system can be reinterpreted as a subsystem of a Hermitian system with higher dimension. In our experiment, we use two 2D subsystems $\mathcal{H}_S$ and $\mathcal{H}_A$, which are expanded by $\{|1\rangle, |2\rangle\}$ and $\{|3\rangle, |4\rangle\}$ to construct a 4-dimensional Hilbert space $\mathcal{H}_S \oplus \mathcal{H}_A$. The unitary operator $U(\alpha, \tau)$ in Eq. (S2) for the 4-dimensional space can be constructed by the Naimark dilation method [2] as

$$U = \begin{pmatrix} F & G \\ -G & F \end{pmatrix}, \tag{S6}$$

where

$$F = \cos(\tau) I_2^m - \mathrm{i}\frac{\Omega}{J}\sin(\tau)\sigma_x^m, \tag{S7}$$

$$G = \frac{\Gamma}{J}\sin(\tau)\sigma_z^m, \tag{S8}$$

I_2^m denotes the 2D identity matrix, and $\sigma_{x,y,z}^m$ are the Pauli matrices.

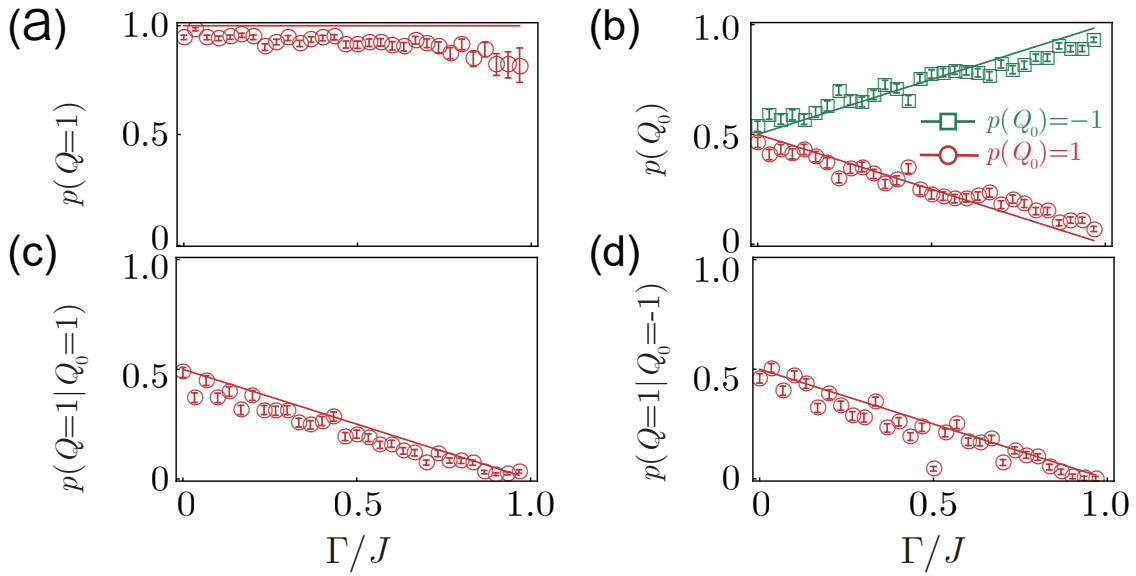

FIG. S3. (color online). Probabilities for obtaining the quantum witness. [(a)-(d)] Measurement results of the probabilities: $p(Q=1)$ (a), $p(Q_0=\pm 1)$ (b), $p(Q=1|Q_0=1)$ (c), and $p(Q=1|Q_0=-1)$ (d) as a function of Γ/J. Error bars represent the standard deviation.

B. Theoretical construction of the metric operator η

Based on the definition of the metric operator η, it should meet the condition

$$\eta\hat{H}_{\mathrm{PT}} - \hat{H}_{\mathrm{PT}}^{\dagger}\eta = 0, \tag{S9}$$

where $\hat{H}_{\mathrm{PT}}^{\dagger}$ is the self-adjoint Hamiltonian of $\hat{H}_{\mathrm{PT}}$ in Eq. (2) of the main text. According to Refs. [2, 12], the metric operator can be easily constructed by taking advantage of the eigenvectors (labeled as $|E_+\rangle$ and $|E_-\rangle$) of $\hat{H}_{\mathrm{PT}}$ and has the form of $\eta = (\Psi\Psi^{\dagger})^{-1}$, where $\Psi = [|E_+\rangle, |E_-\rangle]$ is the constructed matrix by arranging the two eigenvectors as columns.

C. Choice of the initial state and the measurement observable

The Hamiltonian we choose is the most typical form for studying quantum $\mathcal{PT}$ dynamics, with which previous works [13–15] have shown the nonuniform dynamics of skewed Rabi oscillations with the choice of the loss or gain state as the initial state, i. e.,

$$|2\rangle \xrightarrow{\text{fast evolution}} |1\rangle \xrightarrow{\text{slow evolution}} |2\rangle \xrightarrow{\text{fast evolution}} |1\rangle \cdots \tag{S10}$$

To enhance QTCs, we require accelerated dynamics in one-way flip, i. e., a state $|\psi_0\rangle$ evolves first slow, then fast to its orthogonal state $|\psi^{\perp}\rangle$. As seen from Eq. (S10), one process that can meet our requirements is: initially prepared as the intermediate state of the $|1\rangle \to |2\rangle$ flip, after that the system evolves first slow, then fast to the intermediate state of the $|2\rangle \to |1\rangle$ flip. By calculations, we can obtain the required initial and final states as $|1\rangle - \mathrm{i}\,|2\rangle$ and $|1\rangle + \mathrm{i}\,|2\rangle$, respectively. Correspondingly, the measurement observable can be chosen as $\hat{\sigma}_y$. Then, the enhancement of QTCs based on these choices can be further analyzed.

V. THEORETICAL DERIVATION OF THE EVOLUTION SPEED AND THE CORRELATION FUNCTIONS

A. Dynamics of the nonlinear von Neumann equation

Non-Hermitian systems have exhibited excellent ability of the acceleration of the quantum state evolution [16]. Such

acceleration effect can be theoretically explored using the Bloch equations. Consider a two-level system governed by the $\mathcal{PT}$-symmetric Hamiltonian,

$$\hat{H}_{\mathrm{PT}} = J\hat{\sigma}_x + \mathrm{i}\Gamma\hat{\sigma}_z, \tag{S11}$$

where $J > \Gamma$ refers to the $\mathcal{PT}$-symmetric unbroken region. Starting from an initial state, the dynamics of the normalized density matrix $\hat{\rho}$ can be described by the following nonlinear von Neumann equation [17]

$$\dot{\hat{\rho}} = -\mathrm{i}J[\hat{\sigma}_x, \hat{\rho}] + \Gamma\{\hat{\sigma}_z, \hat{\rho}\} - 2\Gamma\hat{\rho}[\mathrm{Tr}(\hat{\sigma}_z\hat{\rho})]. \tag{S12}$$

The density matrix $\hat{\rho}$ is $\hat{\rho} = (\hat{I} + \vec{r}\cdot\vec{\hat{\sigma}})/2$, where the Bloch vector $\vec{r} = (r_x, r_y, r_z) = (\langle\hat{\sigma}_x\rangle, \langle\hat{\sigma}_y\rangle, \langle\hat{\sigma}_z\rangle)$. Then based on Eq. (S12), the Bloch equations can be derived as:

$$\begin{aligned} \dot{r}_x &= -2\Gamma r_x r_z, \\ \dot{r}_y &= -2(Jr_z + \Gamma r_y r_z), \\ \dot{r}_z &= 2(Jr_y - \Gamma r_z^2 + \Gamma). \end{aligned} \tag{S13}$$

In the $\mathcal{PT}$-symmetric unbroken region, when the initial state is chosen as $|-\rangle_y$, the analytical solution for the above Bloch equations can be found as:

$$\begin{aligned} r_x &= 0, \\ r_y &= -\frac{\Gamma + J\cos(2\tau)}{J + \Gamma\cos(2\tau)}, \\ r_z &= -\frac{\sqrt{J-\Gamma}\sqrt{J+\Gamma}\sin(2\tau)}{J + \Gamma\cos(2\tau)}, \end{aligned} \tag{S14}$$

where $\tau = t\sqrt{J^2 - \Gamma^2}$ is the scaled time. And when the initial state is $|+\rangle_y$, the analytical solution has the form of:

$$\begin{aligned} r_x &= 0, \\ r_y &= \frac{\Gamma - J\cos(2\tau)}{-J + \Gamma\cos(2\tau)}, \\ r_z &= \frac{\sqrt{J-\Gamma}\sqrt{J+\Gamma}\sin(2\tau)}{J - \Gamma\cos(2\tau)}. \end{aligned} \tag{S15}$$

The dynamics of the Bloch vector described by Eq. (S14) manifests the acceleration effect of the $\mathcal{PT}$-symmetric qubit as shown in Fig. 3.

B. Evolution speed of the $\mathcal{PT}$-symmetric qubit

For two pure qubit states $|\psi\rangle$ and $|\phi\rangle$, the Fubini-Study metric is defined as

$$s = \arccos(|\langle\psi|\phi\rangle|). \tag{S16}$$

When preparing the initial state in $|-\rangle_y$, the normalized quantum state governed by the $\mathcal{PT}$-symmetric Hamiltonian $\hat{H}_{\mathrm{PT}}$ can be written as

$$|\psi(\tau)\rangle = -\frac{\sqrt{J-\Gamma}\sin(\tau)}{\sqrt{J+\Gamma\cos(2\tau)}}|+\rangle_y + \frac{\sqrt{J+\Gamma}\cos(\tau)}{\sqrt{J+\Gamma\cos(2\tau)}}|-\rangle_y. \tag{S17}$$

Using $s = \arccos(|\langle\psi(\tau)|-\rangle_y|)$, the evolution speed can be derived as

$$v = \frac{\mathrm{d}s}{\mathrm{d}\tau} = \frac{\left|J^2 - \Gamma^2\right|}{\left|\sqrt{J^2-\Gamma^2}(J + \Gamma\cos(2\tau))\right|}. \tag{S18}$$

In the experiment, the states obtained are usually mixed. In this case, the Fubini-Study metric for two density matrices ρ_1 and ρ_2 are computed as

$$s = \arccos\left(\mathrm{Tr}\sqrt{\sqrt{\rho_1}\rho_2\sqrt{\rho_1}}\right). \tag{S19}$$

In Fig. 3(d) of the main text, s is indirectly obtained from the data of the Bloch vectors (r_x, r_y, r_z) [as shown in Figs. 3(a)-3(c)] via Eq. (S19). The error propagation formula can be calculated as

$$\Delta s = \frac{\Delta r_y}{2\sqrt{1-|r_y|^2}}. \tag{S20}$$

Because $r_y(\tau \to 0) = -1$, the coefficient $\frac{1}{2\sqrt{1-|r_y|^2}}$ is very large in this limit. Thus, a significant deviation from the theory appear for $\tau \to 0$ in Fig. 3(d).

C. Analytical forms of the correlation functions

Using the results of Eqs. (S14) and (S15), the analytical forms for the conditional probabilities can be expressed as:

$$\begin{aligned}
p_{_T}(+|+) &= \frac{(J-\Gamma)\cos^2(\tau)}{J-\Gamma\cos(2\tau)},\\
p_{_T}(-|+) &= \frac{(J+\Gamma)\sin^2(\tau)}{J-\Gamma\cos(2\tau)},\\
p_{_T}(+|-) &= \frac{(J-\Gamma)\sin^2(\tau)}{J+\Gamma\cos(2\tau)},\\
p_{_T}(-|-) &= \frac{(J+\Gamma)\cos^2(\tau)}{J+\Gamma\cos(2\tau)},\\
p_{_{2T}}(+|-) &= \frac{(J-\Gamma)\sin^2(2\tau)}{J+\Gamma\cos(4\tau)},\\
p_{_{2T}}(-|-) &= \frac{(J+\Gamma)\cos^2(2\tau)}{J+\Gamma\cos(4\tau)}.
\end{aligned} \tag{S21}$$

Then the two-time correlation functions can be obtained as

$$\begin{aligned}
C_{12} &= p_{_T}(-|-) - p_{_T}(+|-) = \frac{\Gamma + J\cos(2\tau)}{J+\Gamma\cos(2\tau)},\\
C_{13} &= p_{_{2T}}(-|-) - p_{_{2T}}(+|-) = \frac{\Gamma + J\cos(4\tau)}{J+\Gamma\cos(4\tau)},\\
C_{23} &= p_{_T}(+|-)p_{_T}(+|+) - p_{_T}(+|-)p_{_T}(-|+) - p_{_T}(-|-)p_{_T}(+|-) + p_{_T}(-|-)p_{_T}(-|-)\\
&= \frac{J\Gamma^2 + \cos(2\tau)\Big\{J(J^2+J\Gamma-\Gamma^2) - \Gamma\cos(2\tau)\big[-J^2+J\Gamma+\Gamma^2+J^2\cos(2\tau)\big]\Big\}}{\big[J-\Gamma\cos(2\tau)\big]\big[J+\Gamma\cos(2\tau)\big]^2}.
\end{aligned} \tag{S22}$$

Finally, the Leggett-Garg parameter is computed as

$$K_3 = C_{12} + C_{23} - C_{13}. \tag{S23}$$

The results of Eq. (S22) apply to the $\mathcal{PT}$-symmetric unbroken region. In the broken region, by solving the Bloch equations Eq. (S13), under the condition $J \le \Gamma$, we can obtain the analytical two-time correlation functions as:

$$\begin{aligned}
C_{12} &= \frac{\Gamma + J\cosh(2\tau)}{J+\Gamma\cosh(2\tau)},\\
C_{13} &= \frac{\Gamma + J\cosh(4\tau)}{J+\Gamma\cosh(4\tau)},\\
C_{23} &= \frac{J\Gamma^2 + \cosh(2\tau)\Big\{J(J^2+J\Gamma-\Gamma^2) - \Gamma\cosh(2\tau)\big[-J^2+J\Gamma+\Gamma^2+J^2\cosh(2\tau)\big]\Big\}}{\big[J-\Gamma\cosh(2\tau)\big]\big[J+\Gamma\cosh(2\tau)\big]^2}.
\end{aligned} \tag{S24}$$

The maximal QTC in our model can be found by numerically maximizing K_3 when varying the measurement interval τ in both the $\mathcal{PT}$-symmetric unbroken and broken regions, as shown in Fig. 4(e) of the main text.

Besides the above results, based on Eqs. (S14) and (S15), we can also derive the analytical form of the quantum witness in the unbroken region,

$$W = \frac{J+\Gamma}{2J}, \tag{S25}$$

which is shown in Fig. 4(f) of the main text.

[1] M. A. Nielsen and I. L. Chuang, *Quantum Computation and Quantum Information, 10th anniversary ed*(Cambridge University Press, Cambridge, 2010) pp. 189-191 .

[2] U. Günther and B. F. Samsonov, Naimark-dilated $\mathcal{PT}$-symmetric brachistochrone, Phys. Rev. Lett. **101**, 230404 (2008).

[3] H. Y. Ku, N. Lambert, F. J. Chan, C. Emary, and F. Nori, Experimental test of non-macrorealistic cat states in the cloud, npj Quantum Inf. **6**, 98 (2020).

[4] R. E. George, L. M. Robledo, O. J. E. Maroney, M. S. Blok, H. Bernien, M. L. Markham, D. J. Twitchen, J. J. L. Morton, G. A. D. Briggs, and R. Hanson, Opening up three quantum boxes causes classically undetectable wavefunction collapse, Proc. Natl. Acad. Sci. USA **110**, 3777 (2013).

[5] T. Zhan, C. Wu, M. Zhang, Q. Qin, X. Yang, H. Hu, W. Su, J. Zhang, T. Chen, Y. Xie, W. Wu, and P. Chen, Experimental violation of the Leggett-Garg inequality in a three-level trapped-ion system, Phys. Rev. A **107**, 012424 (2023).

[6] F. Jelezko, T. Gaebel, I. Popa, A. Gruber, and J. Wrachtrup, Observation of coherent oscillations in a single electron spin, Phys. Rev. Lett. **92**, 076401 (2004).

[7] T. P. Harty, D. T. C. Allcock, C. J. Ballance, L. Guidoni, H. A. Janacek, N. M. Linke, D. N. Stacey, and D. M. Lucas, High-fidelity preparation, gates, memory, and readout of a trapped-ion quantum bit, Phys. Rev. Lett. **113**, 220501 (2014).

[8] J. A. Jones, Quantum computing with NMR, Prog. Nucl. Mag. Res. Spect. **59**, 91 (2011).

[9] R. H. Hadfield, Single-photon detectors for optical quantum information applications, Nat. Photonics **3**, 696–705 (2009).

[10] C. M. Li, N. Lambert, Y. N. Chen, G. Y. Chen, and F. Nori, Witnessing quantum coherence: from solid-state to biological systems, Sci. Rep. **2**, 885 (2012).

[11] G. C. Knee, M. Marcus, L. D. Smith, and A. Datta, Subtleties of witnessing quantum coherence in nonisolated systems, Phys. Rev. A **98**, 052328 (2018).

[12] C. M. Bender, D. C. Brody, and H. F. Jones, Scalar quantum field theory with a complex cubic interaction, Phys. Rev. Lett. **93**, 251601 (2004).

[13] W. C. Wang, Y. L. Zhou, H. L. Zhang, J. Zhang, M. C. Zhang, Y. Xie, C. W. Wu, T. Chen, B. Q. Ou, W. Wu, H. Jing, and P. X. Chen, Observation of $\mathcal{PT}$-symmetric quantum coherence in a single-ion system, Phys. Rev. A **103**, L020201 (2021).

[14] L. Ding, K. Shi, Q. Zhang, D. Shen, X. Zhang, and Z. W., Experimental determination of $\mathcal{PT}$-symmetric exceptional points in a single trapped ion, Phys. Rev. Lett. **126**, 083604 (2021).

[15] Y. Wu, W. Liu, J. Geng, X. Song, X. Ye, C. K. Duan, X. Rong, and J. Du, Observation of parity-time symmetry breaking in a single-spin system, Science **364**, 878 (2019).

[16] C. M. Bender, D. C. Brody, H. F. Jones, and B. K. Meister, Faster than Hermitian quantum mechanics, Phys. Rev. Lett. **98**, 040403 (2007).

[17] D. C. Brody and E. M. Graefe, Mixed-state evolution in the presence of gain and loss, Phys. Rev. Lett. **109**, 230405 (2012).